TECHNICAL PAPER

ISSN:1047-3289 *J. Air & Waste Manage. Assoc.* **59**:196–206
DOI:10.3155/1047-3289.59.2.196

Transport Mechanisms of Coarse, Fine, and Very Fine Particulate Matter in Urban Street Canopies with Different Building Layouts

Tsang-Jung Chang, Hong-Ming Kao, Yu-Ting Wu, and Wei-Hua Huang
Department of Bioenvironmental Systems Engineering, National Taiwan University, Taipei, Taiwan, Republic of China

ABSTRACT

A particulate matter (PM) transport model is developed to investigate coarse PM (PM_{10}), fine PM ($PM_{2.5}$), and very fine PM (PM_1) transport mechanisms in urban street canopies under low-wind conditions. Two common building layouts (i.e., the open and staggered street canopies) are considered. Large eddy simulations with the subgrid-scale stress model and the wall function are used to simulate urban street-canopy flows. The Lagrangian particle tracking approach, considering the effects of the drag force, gravitational force, Brownian motion, and Saffman lift force on particles is adopted to study PM transport behaviors in urban street canopies. The box counting method is used to calculate the canopy-averaged $PM_{10}/PM_{2.5}/PM_1$ mass concentrations and transport mechanisms at each tracking time. The simulated results show that the removal efficiencies of PM_{10}, $PM_{2.5}$, and PM_1 in the open street canopies are all better than those in the staggered street canopies. As a result, the open street canopies having higher PM removal ability lead to a swifter shift of the particle size distributions towards smaller size and less deviation than the staggered street canopies. The major particle removal mechanism for the open street canopies is particle escape, whereas wall deposition plays the most important role for the staggered street canopies. In comparison with the effectiveness of $PM_{10}/PM_{2.5}/PM_1$ removal for both building layouts, PM_{10} particles are easier to overcome the root mean square vertical turbulent velocity and need less time to deposit. Fine particles would follow airflow paths and need longer time to deposit. As a result, $PM_{2.5}$ and PM_1 are more difficult to be removed than PM_{10}.

IMPLICATIONS

In many Asian cities, an extensive transportation system is built within narrow streets with clusters of buildings. Polluted $PM_{10}/PM_{2.5}/PM_1$ are easily congregated to deteriorate air quality around urban street canopies, leading to urbanites with a high potential for disorders of the respiratory system, especially at low wind speeds. Therefore, there is a high demand in Asia for investigating $PM_{10}/PM_{2.5}/PM_1$ transport mechanisms under low wind speed conditions. This work numerically investigates the canopy airflow patterns and $PM_{10}/PM_{2.5}/PM_1$ transport mechanisms of the open and staggered street canopies. The results will help in understanding PM transport behaviors in urban street canopies.

INTRODUCTION

In urban areas, one of the major sources of air pollution is the airborne particulate matter (PM) emitted from motor vehicle exhaust. PM mostly disperses with canopy airflows around urban streets, and not only generates inferior air quality but also causes injury to the human respiratory system. Several studies have indicated that coarse PM (PM_{10}, aerodynamic diameters less than 10 μm) can be inhaled and deposited in the human respiratory system to cause serious long-term health effects such as cardiovascular disease or acute health effects such as allergies and irritation of the eyes, nose, and throat.[1,2] In particular, the finer particle fractions of PM_{10} such as $PM_{2.5}$ (fine PM) and PM_1 (very fine PM) can penetrate deeper into the pulmonary alveolus and therefore cause an increase in daily mortality and asthma.[3–5] In many Asian cities, such as Taipei, Tokyo, Shanghai, and Hong Kong, extensive transportation systems are built within narrow streets with clusters of buildings or skyscrapers. PM_{10}, $PM_{2.5}$, and PM_1 are easily congregated to deteriorate air quality around urban street canopies, causing city dwellers to have a high potential for a disorder of the respiratory system, especially at low wind speed conditions. Thus, studies on transport behavior and mechanism of PM_{10}, $PM_{2.5}$, and PM_1 at low wind speed conditions are crucial in Asia to promote a more comfortable and healthy urban pedestrian environment.

Academic researches regarding PM transport behavior and mechanism in urban areas have been carried out by full-scale experiments,[6–8] wind tunnel experiments,[8–11] and microscale numerical studies.[12–24] Generally, experimental studies can provide useful knowledge of pollutant dispersion and PM transport behavior on the sample points for given experimental configurations. It is very difficult to simultaneously obtain temporal and spatial information on the distributions of airflow velocity, PM size, and concentration for the entire urban areas. With increased computing power, microscale computational fluid dynamics (CFD) are capable and convenient for analyzing airflow patterns and PM concentrations because CFD models can reproduce the entire flow and concentration fields over a street-canopy domain rather than at specific points.

PM transport behaviors and mechanisms in urban areas are influenced by many factors, such as inflow conditions (wind speed, wind direction and turbulence), building geometry (height, width, roof type), surrounding

building layouts (street width and configuration), thermal stratification (solar insulation and orientation, building and street thermal capacitance), and traffic conditions (traffic intensity, vehicle emissions, vehicle movement). One potential advantage of the use of microscale CFD is that CFD models can provide an opportunity to examine the effects of the above various factors individually, which can directly improve the understanding of PM transport behavior and mechanisms in urban street canopies. Among the microscale CFD studies[12–24] (e.g., Walton and Cheng,[12] Walton et al.,[13] and Caton et al.[14]) have used large eddy simulations to investigate pollutant dispersion mechanisms within an isolated urban street canyon. Lee and Park[15] and So et al.[16] have studied wind flow and pollutant dispersion in a two-dimensional (2D) street canyon with different aspect ratios. Xie et al.[17] conducted investigations on the effect of solar radiation on pollutant distribution in an urban street canyon. Xia and Leung[18] and Chang and Wu[19] used the Lagrangian particle model together with a 2D wind field model to simulate particle dispersion for different building configurations within urban street canopies. Liu and Ahmadi[20] and Ahmadi and Li[21] developed a Lagrangian particle tracking model to study PM transport behaviors near Peace Bridge, Buffalo, NY, and an isolated building, respectively. Seven particle sizes (50, 20, 10, 5, 1, 0.1, and 0.01 μm) were used to investigate the relationship between particle size and PM transport and deposition behavior. However, these works did not integrate their results of various single-size particles into $PM_{10}/PM_{2.5}/PM_1$ transport mechanisms. For researches regarding pollutant dispersion and PM transport behaviors around urban street canopies with different building layouts, some pioneer works like Hanna et al.,[22] Cheng et al.,[23] and Zhang et al.[24] have only reported the three-dimensional (3D) canopy airflow patterns of the open and staggered street canopies. Their works did not extend to analyzing $PM_{10}/PM_{2.5}/PM_1$ transport mechanisms in urban street canopies with different building layouts. To fill this gap, the study presented here investigates the canopy airflow patterns and $PM_{10}/PM_{2.5}/PM_1$ transport mechanisms in urban street canopies with different building layouts under low wind speed conditions.

METHODOLOGY

The numerical methodology for investigating $PM_{10}/PM_{2.5}/PM_1$ transport mechanisms in urban street canopies consists of the 3D Eulerian street-canopies flow model and the 3D Lagrangian particle tracking model. The street-canopies flow model firstly conducts the large eddy simulations (LES) of the Eulerian turbulent flows, in which wind velocities and pressure are obtained by solving the time-dependent Navier–Stokes equations. Next, the particle tracking model adopts the Lagrangian scheme to determine PM trajectories. Finally, the box counting method is used to calculate the canopy-averaged $PM_{10}/PM_{2.5}/PM_1$ mass concentrations at each tracking time by analyzing the calculated PM trajectories at each time step.

3D Eulerian Street-Canopies Flow Model

Because of the rapid advance in computational facilities, microscale CFD has received more and more attention and has successfully been applied to several wind engineering problems in street canopies.[20–24] Generally, a fully developed turbulent flow within urban street canopies contains eddies of many length scales. The study presented here utilizes LES to investigate the turbulent canopy flow. When LES filtering is applied, large eddies are directly solved in the computational grid and small eddies are filtered out to the subgrid-scale Reynolds stress without being neglected.[25,26] The filtered equations of mass and momentum in LES can be expressed in the following:

$$\frac{\partial \bar{u}_i}{\partial x_i} = 0 \tag{1}$$

$$\frac{\partial \bar{u}_i}{\partial \tau} + \frac{\partial \bar{u}_i \bar{u}_j}{\partial x_j} = -\frac{1}{\rho}\frac{\partial \bar{p}}{\partial x_i} + \frac{\partial}{\partial x_j}\left((\nu + \nu_t)\left(\frac{\partial \bar{u}_i}{\partial x_j} + \frac{\partial \bar{u}_j}{\partial x_i}\right)\right) \tag{2}$$

$$\nu_t = (C_s\bar{\Delta})^2\,(2\tilde{S}_{ij}\cdot\tilde{S}_{ij})^{1/2} \tag{3}$$

where $\bar{u}_i$ is the component of filtered instantaneous fluid velocity in the x_1 direction, $\bar{p}$ is air pressure, t is time, ρ is air density, ν is air kinematic viscosity, ν_t is subgrid eddy viscosity, $\bar{\Delta} = (\Delta x \Delta y \Delta z)^{1/3}$ is the filter length scale, and $\tilde{S}_{ij}$ is the fluid strain rate. In eq 3, C_s, a Smagorinsky constant usually between 0.1 and 0.2,[25] is 0.15 in the study presented here. The bar "–" is spatial grid filtering. The LES is primarily valid for turbulent core flows (i.e., the flow in the regions somewhat far from walls).[25] Thus, the wall function model[27] near the solid boundary and the non-slip boundary on the wall are adopted as well. The study presented here uses the finite volume method. The numerical details can be found in Chang et al.[28,29] It should be noted that because solving eqs 1–3 produces the time-dependent velocity, the time-averaged velocity $\langle\bar{u}_i\rangle$ can be acquired from the statistic analysis of the instantaneous velocities $\bar{u}_i$ according to $\bar{u}_i = \langle\bar{u}_i\rangle + \bar{u}_i'$, where $\bar{u}_i'$ denotes the component of filtered turbulent velocities.

Three kinds of flow boundary conditions are adopted, including the inflow boundary, outflow boundary, and wall boundary. At the inflow boundary, the inflow velocity is in power-law profile and remains unchanged with time. At the outflow and upper boundaries, the velocity gradient is set to be zero. The non-slip boundary is applied to all building walls, roofs, and ground.

3D Lagrangian Particle Tracking Model

In the study presented here, a Lagrangian scheme is selected to record all positions of PM transport at each time step. A series of aerial snapshots of the particle movement are used to generate continuous pictures of the trajectory simulations. The PM size range that we focus on is particle diameters less than 10 μm (PM_{10}). Under such PM size range, several particle driving forces have to be considered: the gravitational force F_G, the drag force F_D, the Saffman lift force F_S, and the Brownian motion force F_B.[30–32] The governing equations are

$$\frac{dx_i^p}{dt} = u_i^p \tag{4}$$

and

$$\frac{1}{6}\pi\rho_p d_p^3 \frac{du_i^p}{dt} = F_G + F_D + F_S + F_B$$

$$= \frac{1}{6}\pi d_p^3 \cdot (\rho_p - \rho) g_i \delta_{i3} - \frac{1}{6}\pi\rho_p d_p^3 \cdot \frac{1}{\tau}(u_i^p - \bar{u}_i) \qquad (5)$$

$$- \frac{1}{6}\pi\rho_p d_p^3 \cdot \frac{5.188\nu^{1/2}\, d_{ij}}{S d_p (d_{lk} d_{kl})^{1/4}} (u_j^p - \bar{u}_j) + \frac{1}{6}\pi\rho_p d_p^3 \cdot G_1 \sqrt{\frac{\pi S_0}{\Delta t}}$$

where x_i^p is the coordinate of particles, u_i^p is particle velocity, ρ_p is particle density, d_p is particle diameter, S is the density ratio between particle and adjacent fluid, δ is the unit Kronecker delta function, Δt is the particle time step, τ is the relaxation time of the particle,[33] and d_{ij} ($= (u_{i,j} + u_{j,i})/2$) is the deformation rate tensor. F_B significantly affects the motion of submicron particles and is simulated as a Gaussian white noise random process with a random variable G_i (zero-mean and unit variance) and an appropriate spectral intensity S_0.[31] Each particle trajectory can be tracked by solving eqs 4 and 5 by using a fourth-order predictor-corrector method. The numerical details can be found in Chang et al.[28]

For the study presented here, several assumptions are made to simplify the simulation of PM transport process without losing its accuracy. The additional hydrodynamic

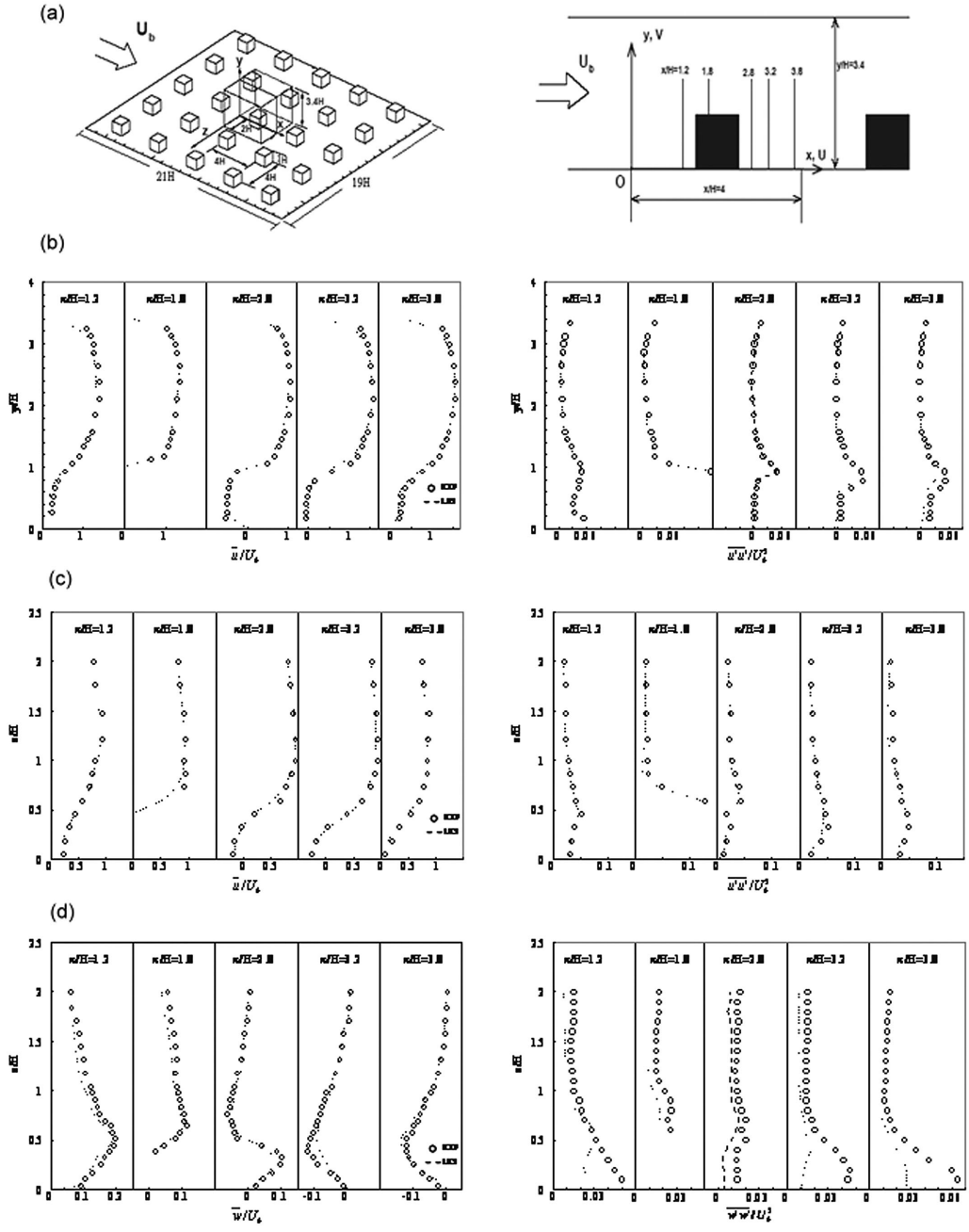

Figure 1. (a) Schematic diagram of the matrix of cubes and the measured locations in the experiment of Meinders and Hanjalic.[34] Time-averaged velocities and Reynolds stresses (b) in the *x* direction on the vertical (*xy*) plane, (c) in the *y* direction, and (d) in the *z* direction on the horizontal (*xz*) plane. The inflow velocity (U_b) is 5 m/sec.

forces (such as virtual mass, Basset, and Faxen) and particle-particle interactions are expected to be small and are neglected. The size of particles is defined by the aerodynamic diameter of particles. Airborne particles have no influence on the surrounding airflow field. There is no heat and mass transfer between particles and air. In the transport process, particle coagulation, electrostatic force, and phase change are not considered.

Two types of particle boundary conditions are herein used, namely the trap boundary and the outflow boundary. The trap boundary means that once a particle touches the non-slip surface boundaries such as the ground, roof, or building walls, the particle is trapped and the particle tracking process is terminated. The outflow boundary is used for the boundaries of the given computational domain. When a particle passes through the outflow boundary, the particle tracking is terminated. It should be noted that, because of the properties of PM and building surfaces used in this study, the critical velocity[33] for which bounce will occur if that velocity is exceeded is larger than the low wind speed condition of 2.5 m/sec herein used. Thus, particle adhesion is a dominant mechanism of particle-surface interaction. This is the reason why we use the trap boundary condition rather than the rebound boundary condition.

Particle Mass Concentration Calculation

On the basis of the above calculated instantaneous particle trajectories at each time step, the particle mass concentrations can be next calculated by using the box counting method.[18] For the box counting method, the entire domain of interest is discretized in control volumes of suitable dimensions and the particle mass concentration is calculated by counting the mass of the Lagrangian particles in these control volumes. Therefore, this method can obtain the

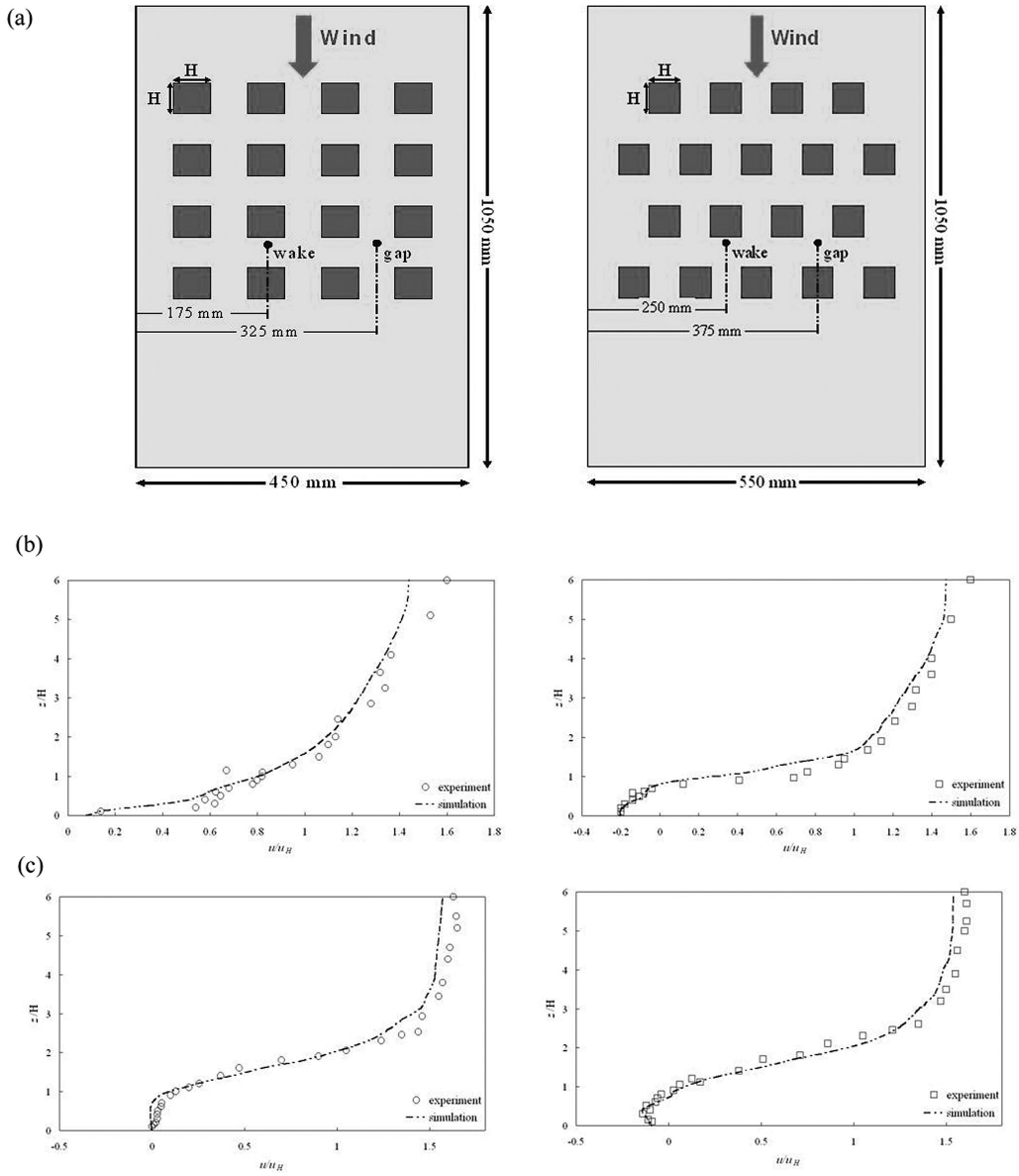

Figure 2. (a) Schematic diagram of the two cubical layouts and the measured locations in the experiment of Macdonald et al.,[35] (b) time-averaged velocities at gap and wake regions of the open street canopies, and (c) time-averaged velocities at gap and wake regions of the staggered street canopies. The inflow velocity u_H is 50.5 mm/sec.

average concentrations of these control volumes and transport mechanisms at each tracking time. In the study presented here, the entire street canopy is regarded as a single control volume. The canopy-averaged $PM_{10}/PM_{2.5}/PM_1$ mass concentrations at each tracking time can be determined by using the following simple expression:

$$C_{ave} = \frac{M_S}{V} \quad (6)$$

where M_S is the total mass of suspended particles in the street canopy, and V denotes the volume of the street-canopy domain.

MODEL VERIFICATION

To ensure the reliability of the 3D street-canopies flow model, model verification is first performed by comparison with the reliably measured airflow velocities of Meinders and Hanjalic.[34] The outline of the cube array used by Meinders and Hanjalic is displayed in Figure 1a. A sum of 25 cubes of side length H is placed in the experimental field with the size of 21 H in length, 19 H in width, and 3.4 H in height. The cube configuration consists of five aligned columns of five cubes, where each has cube spacing of 3 Hr in the x and z direction. The inflow velocity is 5 m/sec. The corresponding Reynolds number based on the height of the cube is 3,800. The time-averaged velocities and the Reynolds stress profiles at five positions shown in Figure 1a were measured. Figure 1, b–d, shows the comparison with the time-averaged velocities and the Reynolds stresses of the x-direction on the vertical (xy) plane, and the y direction and z direction on the horizontal (xz) plane. The agreement between the numerical results and experimental measurement is quite satisfactory.

The study presented here is next validated by the hydraulic flume experiment of Macdonald et al.[35] In this experiment, two cubical layouts of the open and staggered array are used as displayed in Figure 2a. The cubic configuration comprises 16 cubes for the open cube array and 18 cubes for the staggered cube array. The height of the cubes is the same as the spacing between two adjacent cubes. The power-law velocity profile of $u(z)/u_H = (z/H)^{0.29}$ at $u_H = 50.5$ mm/sec is adopted as the velocity of the incoming flow. The airflow velocity profiles at gap and wake for each cube array shown in Figure 2a were measured. Figure 2, b and c, shows the comparison with the time-averaged velocity profiles between the numerical and experimental results at gap and wake for the open and staggered cube array. The numerical results are also in good agreement with the experimental measurement.

DESCRIPTIONS OF NUMERICAL SCENARIO SIMULATIONS

Case Specification

The study case considered in the research presented here is located in Downtown Taipei. Two building layouts commonly seen in Taipei city (i.e., the open and staggered street canopies) are considered to investigate the effect of different building layouts on $PM_{10}/PM_{2.5}/PM_1$ transport mechanisms. The height of all the buildings (H) is set as 25 m, which is approximately seven to eight stories. The widths of all of the streets are also 25 m. The open and staggered street canopies are the same as the experiment of Macdonald et al.[35] with the scale of 500 to 1. The geometrical configuration is displayed in Figure 3. The computational domain for 3D flow field and particle trajectory tracking is approximately $525 \times 225 \times 150$ m for the open street canopies, and $525 \times 275 \times 150$ m for the staggered street canopies. Furthermore, the major interest of the study is to investigate the transport mechanisms of size-dependent PM with different building layouts in urban street canopies. Some simplifications have been made in the numerical simulations. The

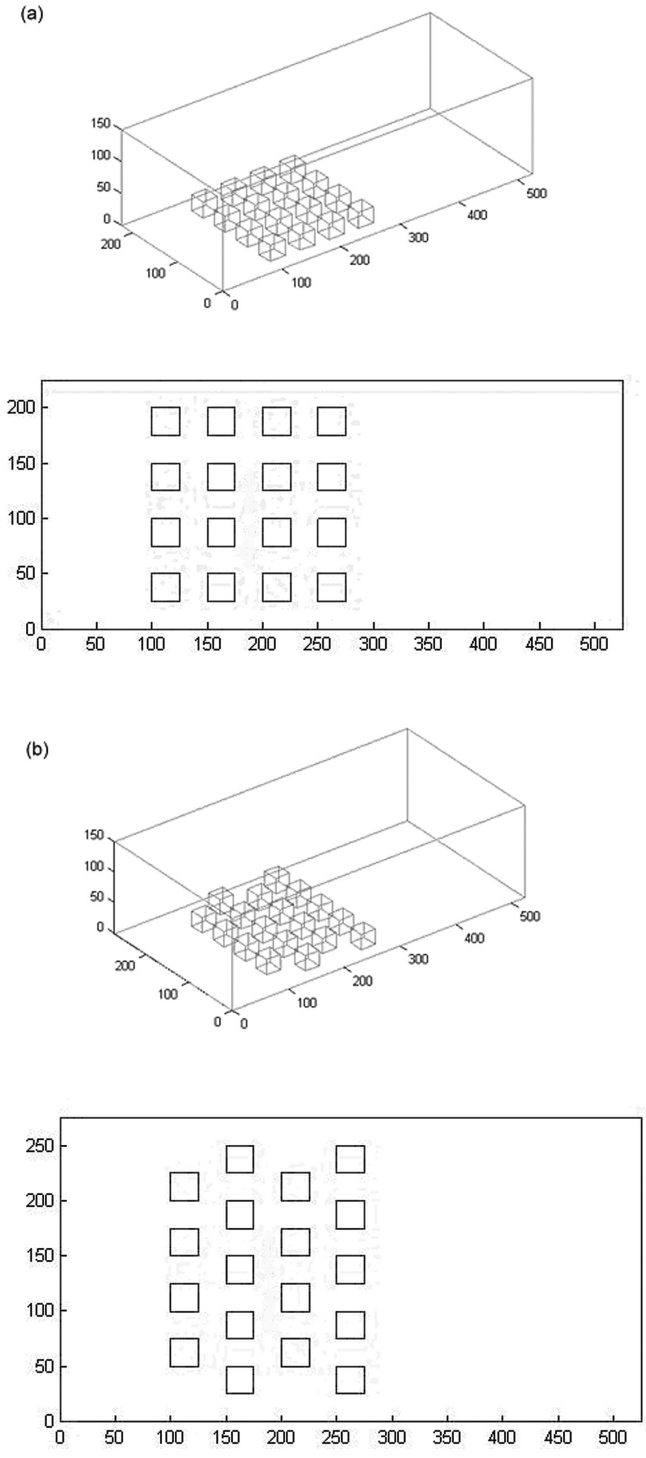

Figure 3. Schematic diagram of the (a) open and (b) staggered street canopies.

isothermal condition with a domain temperature of 20 °C is assumed. The incoming velocity is in power-law profile of $u(z)/u_H = (z/H)^{0.29}$ with a low-wind condition of $u_{H=25m}$ = 2.5 m/sec. The perpendicular wind direction to building walls only is considered.

A PM_{10} profile was measured in Downtown Taipei in 2005 under a similar wind condition as the current numerical simulations by using a portable laser dust monitor (Series 1100, Grimm Labortechnik GmbH & Co. KG). The measured PM_{10}, $PM_{2.5}$, and PM_1 mass concentrations are 48.1, 24.4, and 14 $\mu g/m^3$, respectively, which are used as the initial PM_{10} mass concentrations. The measured profile, following a lognormal distribution with a geometric mean diameter (GMD) of 1.09 μm and a geometric standard deviation (GSD) of 1.27, is adopted as the initial PM_{10} size profile. The profile is separated into ten size groups from aerodynamic diameter ranging from 0.5 to 10 μm (see Table 1). The PM concentration is considered as a constant in each size group. The particle mass carried by each sample particle for each size group can be seen in Table 1.[29] In Figure 4, the initial PM_{10} is instantaneously released in the major road, which is situated in the upwind direction of the buildings. Particles are uniformly and statically distributed over the major road space with a volume source of 25 × 225 × 5 m for the open street canopies and 25 × 275 × 5 m for the staggered street canopies. The height of the release (5 m) is determined by the observed fact in the study site that high PM_{10} levels have been observed at the window of the second floor (~5 m high) of the building in front of the major road. The street-canopy domain is defined as 230 × 225 × 30 m (see Figure 4) for the open street canopies, and 230 × 275 × 30 m for the staggered street canopies. The above domains are for the purpose of calculating the canopy-averaged particle mass concentrations at each tracking minute as shown in eq 6 and the PM_{10} transport mechanisms in Table 2. Three widely used particle size indexes of PM_1, $PM_{2.5}$, and PM_{10} are determined by numerically integrating the appropriately weighted moment of the respective particle size group.

Particles are driven into buildings by the incoming wind, resulting in the redistribution of PM concentrations in the open or staggered street canopies. The box counting method is next used to calculate the canopy-averaged mass concentrations at each time step. The time variations of $PM_{10}/PM_{2.5}/PM_1$ canopy-averaged mass concentrations within the entire street-canopy domain (see Figure 4) can be calculated by using the simulated results of particle trajectories together with the average particle concentration equation in eq 6.

It is important to note that in the study presented here, after carrying out the LES procedure for several flow-through times to ensure that the final time-averaged results are independent of the initial conditions, the time-averaged velocities and turbulent statistics are collected over 600 sec. In the Lagrangian particle tracking process, the determination of time step size in the study presented here depends on the particle diameter. The time step is selected as one order smaller than the relaxation time of particles. Six hundred ensembles are undertaken to obtain the ensemble-averaged trajectories for each sample particle at each time step.

Sensitivity Analysis of Grid and Particle Number

In CFD, the numerical accuracy depends on the numerical schemes, boundary conditions, grid resolutions, etc. Before conducting the numerical simulations of the study case, the grid sensitivity analysis is performed to evaluate the numerical discretization errors and the suitable grid density that can reach an acceptable value. Four grid resolution tests from coarse to fine (ranging from 100,000, 300,000, and 500,000 to 1,000,000 grids) are used to establish the grid density necessary to ensure grid-independent solutions. The scaled residual value of 10^{-4} is used for all variables. The results show that the solutions are convergent when the grid number exceeds 500,000. Consequently, to reach a balance between adequate numerical accuracy and acceptable computation expense, this study uses 500,000 grids to carry out the airflow computation.

In the Lagrangian scheme, the PM mass concentrations are generally determined by the statistical analysis of the trajectories of the particles. By using the abovementioned 500,000 grids, particle number sensitivity analysis is next performed. The study presented here chooses three particle sizes of 10, 5, and 1 μm diameter to perform the sensitivity analysis for the open and staggered street canopies. For each particle size, four particle numbers of 100, 500, 1000, and 2000 particles are tested. The results show that the more number of particles released, the more stable are the PM mass concentrations. The solutions are convergent as the particle number exceeds 1000. To balance satisfactory numerical accuracy and suitable computational time, the optimal number of the released sample particles for each particle size is 1000. As a result, the total sample particles required for the ten size groups in the study presented here is thus 10,000 (see Table 1).

RESULTS AND DISCUSSION

Airflow and Particle Transport between Buildings

The instantaneous and time-averaged airflow velocities of the 500,000 nonuniform grids are obtained by solving eqs

Table 1. Particle mass distributed in each PM size group (10,000 sample particles).

	(1)	(2)	(3)	(4)	(5)	(6)	(7)	(8)	(9)	(10)
Size range (μm)	0.5–1	1–2	2–3	3–4	4–5	5–6	6–7	7–8	8–9	9–10
Average diameter (μm)	1	1.5	2.5	3.5	4.5	5.5	6.5	7.5	8.5	9.5
Open street canopies										
Particle mass carried by each sample particle (μg)	49.10	24.90	23.04	14.24	11.78	10.74	10.14	9.32	7.94	7.90
Staggered street canopies										
Particle mass carried by each sample particle (μg)	60.02	30.43	28.16	17.40	14.40	13.13	12.39	11.39	9.70	9.65

Notes: PM_1 mass concentration= [total mass of (1)]/canopy volume; $PM_{2.5}$ mass concentration= [total mass of (1) + (2) + 0.5 × (3)]/canopy volume; PM_{10} mass concentration = [total mass of (1) + (2) + (3) +...+ (10)]/canopy volume

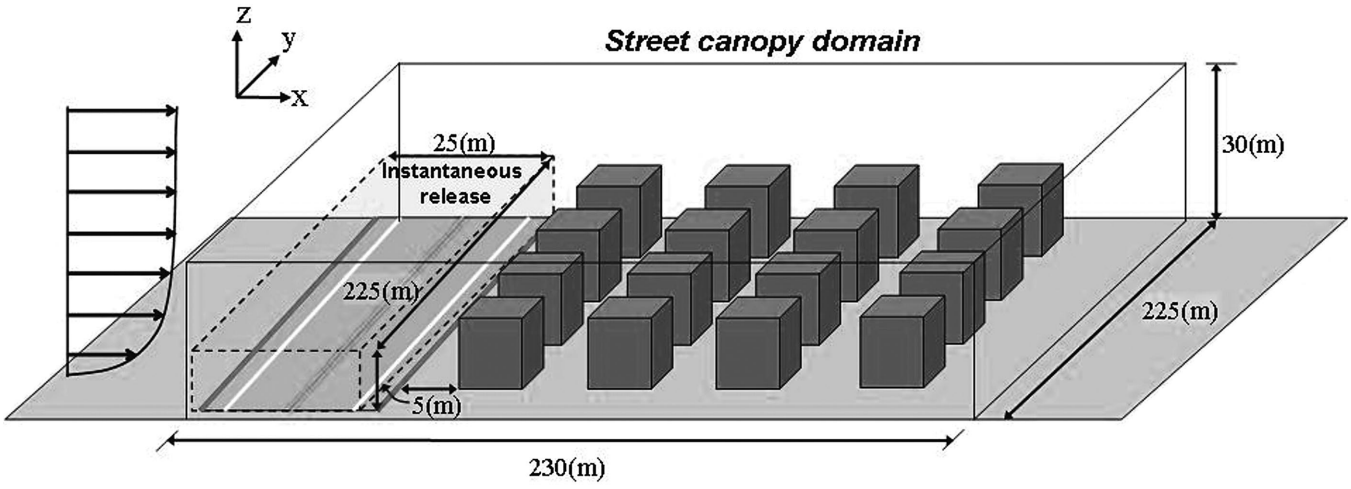

Figure 4. Schematic diagram of the initial condition of the instantaneous particle release.

1–3. To demonstrate the airflow characteristics of the open and staggered street canopies, two representative planes at the pedestrian level (z = 1.5 m [xy plane] and y = 137.5 m [xz plane]), as shown in Figure 5, are chosen to display the airflow patterns of the street canopies. In Figure 5a, for the open street canopies, the incoming flows from the main street are impeded by the first column of the buildings so that the canopy flows go straightforwardly along the streets of the aligned buildings, leading to the strong jet flows in the gap (street) region and the weak eddy flows in the wake region. On the other hand, in Figure 5b, the canopy flows are subject to the blockage of the staggered buildings so that the airflow paths have to skirt around the buildings, resulting in a pair of counter-rotating vortexes in the back of the buildings. In Figure 5, c and d, the airflow pattern of the open street canopies is skimming flows, whereas the airflow pattern of the staggered street canopies looks like wake interference flows. Thus, the wake region in the open street canopies receives less air exchange than that in the staggered street canopies.

The side-view snapshots of 5-μm PM trajectories in the open and staggered street canopies for various particle tracking times are shown in Figure 6. One can clearly see particle dispersion behaviors in both of the street canopies. For the open street canopies, particles are driven by the unimpeded canopy flows so that particles are straightforwardly moving from the upwind to downwind buildings. In the case of the staggered street canopies, particles are hindered by the buildings, resulting in more particle deposition on the building walls.

Canopy-Averaged PM_{10}, $PM_{2.5}$, and PM_1 Mass Concentrations

On the basis of the above calculated PM trajectories, the canopy-averaged $PM_{10}/PM_{2.5}/PM_1$ concentrations are obtained by using eq 6. Figure 7 gives the time variations of the canopy-averaged $PM_{10}/PM_{2.5}/PM_1$ mass concentrations for the open and staggered street canopies. In the case of the open street canopies, particles are driven through the unimpeded canopy flows. All of PM_{10}, $PM_{2.5}$, and PM_1 mass concentrations are substantially reduced because of the large ventilated areas. At the 15th minute of the particle tracking time, almost all of the particles are cleaned out. For the staggered street canopies, the unimpeded canopy airflow only occurs in the first column of the buildings so that good PM removal can only be seen in this area. The rest of the canopy space is poorly ventilated, in which particles are not easily removed, resulting in poor PM removal. Because of the small ventilated areas, all of the PM_{10}, $PM_{2.5}$, and PM_1 mass concentrations cannot be effectively reduced compared with the open street canopies. PM_{10} $PM_{2.5}$, and PM_1 mass concentrations are still 23, 28, and 30%, respectively, of the initial concentrations at the 15th minute.

Moreover, it can also be observed from Figure 7 that PM_{10} mass concentrations in both of the street canopies quickly decline with time. However, $PM_{2.5}$ and PM_1 mass

Table 2. PM_{10} transport mechanisms for the open and staggered street canopies (%)

	Open Street Canopies				Staggered Street Canopies			
Time (min)	Escape	Wall Deposition	Ground Deposition	Roof Deposition	Escape	Wall Deposition	Ground Deposition	Roof Deposition
1	16.7	5.5	12.6	0.0	5.5	10.8	6.7	0.0
3	25.4	11.7	17.9	0.0	9.7	22.4	10.4	0.0
5	34.3	12.9	21.5	0.0	12.4	35.3	11.3	0.0
7	38.9	14.6	23.0	0.1	12.8	36.2	12.6	0.0
10	45.0	15.9	25.3	0.2	16.4	37.0	13.4	0.2
15	56.3	16.5	26.1	0.3	22.3	38.5	16.3	0.2

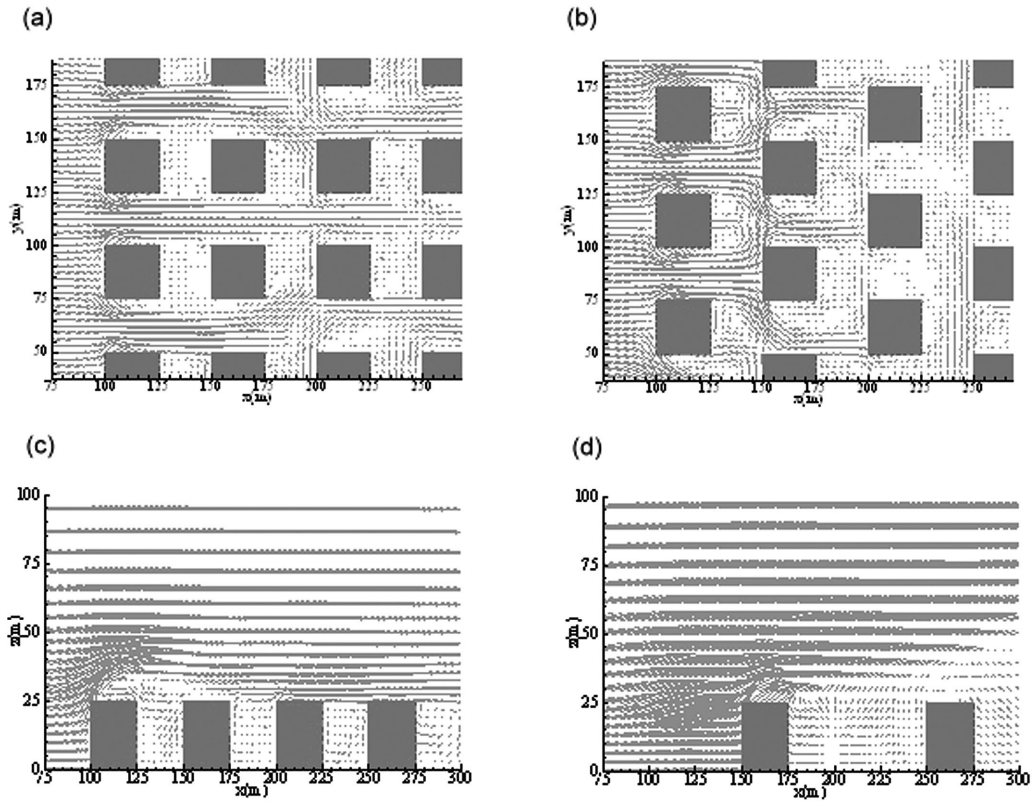

Figure 5. Time-averaged velocities at $z = 1.5$ m for the (a) open and (b) staggered street canopies, and at $y = 137.5$ m for the (c) open and (d) staggered street canopies.

concentrations are relatively slowly decreasing. Obviously PM_{10} is easier to remove compared with $PM_{2.5}$ and PM_1. This result is reasonable because coarse particles (>2.5 μm), possessing larger inertia and relaxation time to maintain their velocities for longer time duration, are easier to drive out of the street canopies than $PM_{2.5}$ through deposition and escape mechanisms. On the contrary, $PM_{2.5}$ particles have smaller inertia and relaxation time, so they are more easily influenced by the complicated airflow patterns within the street canopies such as incoming momentum jets, various length-scale vortexes, and diverging/converging/circulating flows, and are thus trapped in the eddies. This phenomenon can result in the accumulation of $PM_{2.5}$ and PM_1 within the street canopies rather than PM_{10}.

It is important to note that $PM_{2.5}$ suspended in street-canopy space is harmful to human health and induces significant influence on the respiratory system of human beings. Therefore, for the purpose of health protection for urban passengers, using PM_{10} level as the only PM index is not enough. $PM_{2.5}$ and PM_1 levels should also be considered. In Taiwan, air quality is monitored through the Taiwan Area Air Quality Monitoring Network (TAQMN), which comprises 74 stationary automatic air quality monitoring stations and 2 mobile monitoring stations. The hourly PM_{10} and $PM_{2.5}$ concentrations are measured. However, the current air pollution control act revised by the Taiwan Environmental Protection Agency in 2002 only regulates PM_{10} as a 24-hr average (125 μm/m^3) and 1-yr average (65 μm/m^3) for air quality standards. Thus, we emphasize the importance of considering $PM_{2.5}$ and PM_1 in addition to PM_{10}.

PM_{10} Transport Mechanisms

In the study presented here, the carried particles are redistributed along with the canopy flows for the two street canopies. During the PM redistribution process, particles would suspend in the air, settle down on the building roof or the ground, inertially impact or intercept on the building walls, or escape out of the simulated domain. The particle transport mechanisms are usually classified into three parts: suspension, escape, and deposition (including ground, roof, and wall deposition). Herein, deposition and escape are regarded as the particle removal mechanisms.[32] The above deposition mechanism represents the combined results of inertial impaction, turbulence-eddy impaction, interception, gravitational sedimentation, and the Brownian motion, which can be thoroughly simulated by the present numerical model.

Table 2 demonstrates the cumulative mass fractions of particle escape, wall deposition, ground deposition, and roof deposition for both of the street canopies. It can be seen from Figure 7 and Table 2 that most particles go along with the unimpeded canopy flow and directly run away from the open street canopies. Particles are effectively removed out of the domain of the street canopies. At the 15th minute of the tracking time, only 1% of PM_{10} is still suspended within the street canopies, and the remaining 99% of PM_{10} is removed by escape (56.3%), wall deposition (16.5%), ground deposition (26.1%), and roof deposition (0.3%). Obviously, particle escape is the most important removal mechanism compared with particle deposition (42.9%). On the other hand, for the staggered street canopies, because of the blockage

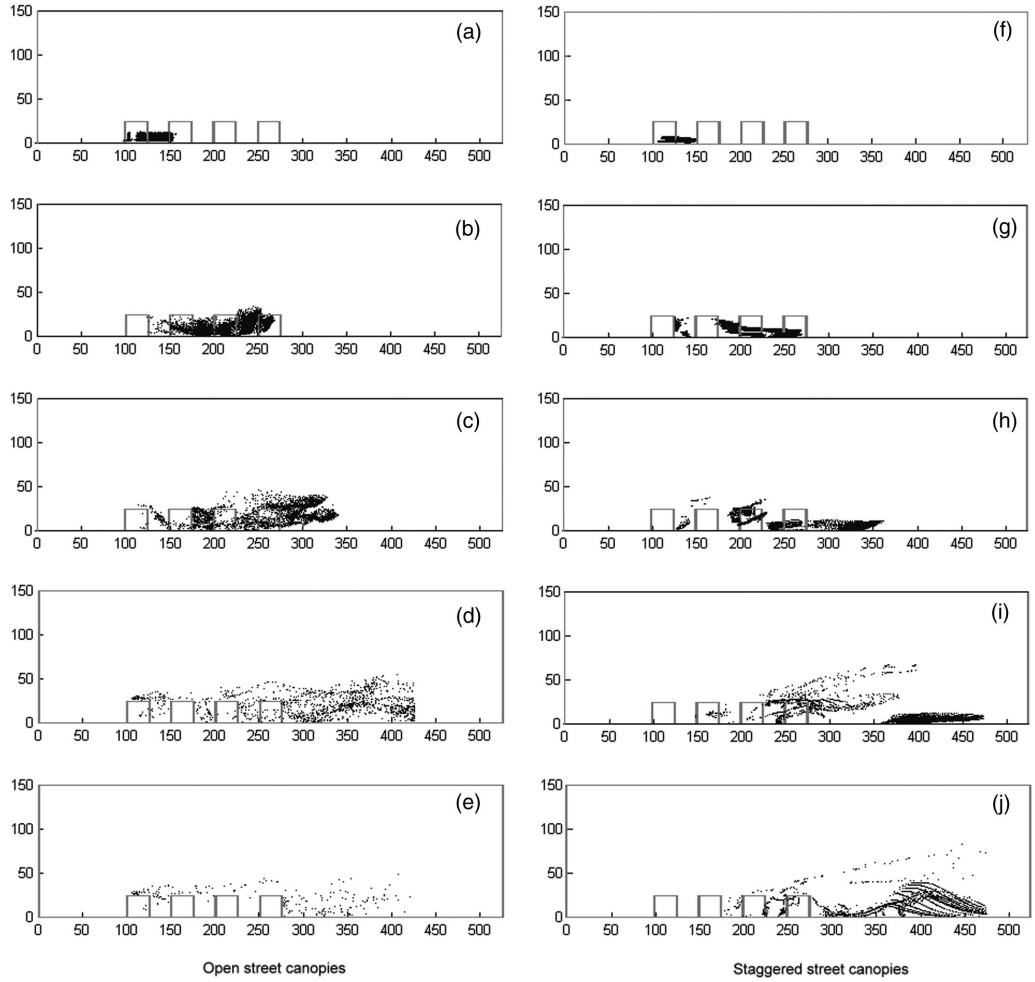

Figure 6. PM transport trajectories in the (a–e) open and (f–j) staggered street canopies at the (a and f) 1st, (b and g) 3rd, (c and h) 5th, (d and i) 10th, and (e and j) 15th min of tracking time.

effect of the buildings, the incoming airflow paths are hindered, resulting in 23% of PM_{10} still being suspended within the street canopies at the 15th minute. Only 77% of PM_{10} is removed, in which wall deposition (38.5%) is the major removal mechanism compared with particle escape (22.3%), ground deposition (16.3%), and roof deposition (0.2%). The cumulative mass fraction of deposited particles (55%) is about as 2.5 times as that of escaped particles. In comparing PM transport mechanisms for the two street canopies, it can be found that the effect of different building layouts not only affects the magnitude of $PM_{10}/PM_{2.5}/PM_1$ mass concentrations, but also changes the particle removal mechanisms under the same inflow condition. Therefore, the building layout is indeed an important factor of PM transport in urban areas.

On the basis of the above results, the study presented here further compares the initial particle size distribution and the particle size distributions at the 1st, 5th, 10th, and 15th minutes of the tracking time for the two street canopies. The GMD and the GSD of the particle size profiles for the open street canopies at the 1st, 5th, 10th, and 15th min are (1.09 μm, 1.26), (1.07 μm, 1.22), (1.01 μm, 1.10), and (1.01 μm, 1.10), respectively; whereas they are (1.09 μm, 1.26), (1.08 μm, 1.24), (1.02 μm, 1.10), and (1.01 μm, 1.10), respectively, for the staggered street canopies. In comparison with the initial condition of (1.09 μm, 1.27), both of the flow patterns of the two street canopies lead to the apparent shift of the particle size distributions towards smaller size and less deviation during the particle tracking process. The open street canopies having higher PM removal ability would result in a swifter shift. In addition, it can be inferred from the above results that, because of the shift of the particle size distribution towards smaller size, PM_{10} is much easier to remove than finer particles like $PM_{2.5}$ and PM_1 for the two street canopies. It should be noted that, because of the measurement limitation of the portable laser dust monitor herein used, the study presented here considers aerodynamic diameters ranging only from 0.5 to 10 μm. As shown in Table 1, there is only one size group of PM_1 in the calculation, which thus provides limited information on PM_1. Further study on PM_1 is desirable.

Finally, in addition to building layouts, $PM_{10}/PM_{2.5}/PM_1$ transport behaviors and mechanisms in urban areas are also affected by inflow conditions, building geometry, and traffic conditions. Further extensive work investigating the effects of the above various factors individually will be useful. In addition, the results of modeling mean and turbulent characteristics of the flow in the study presented here were

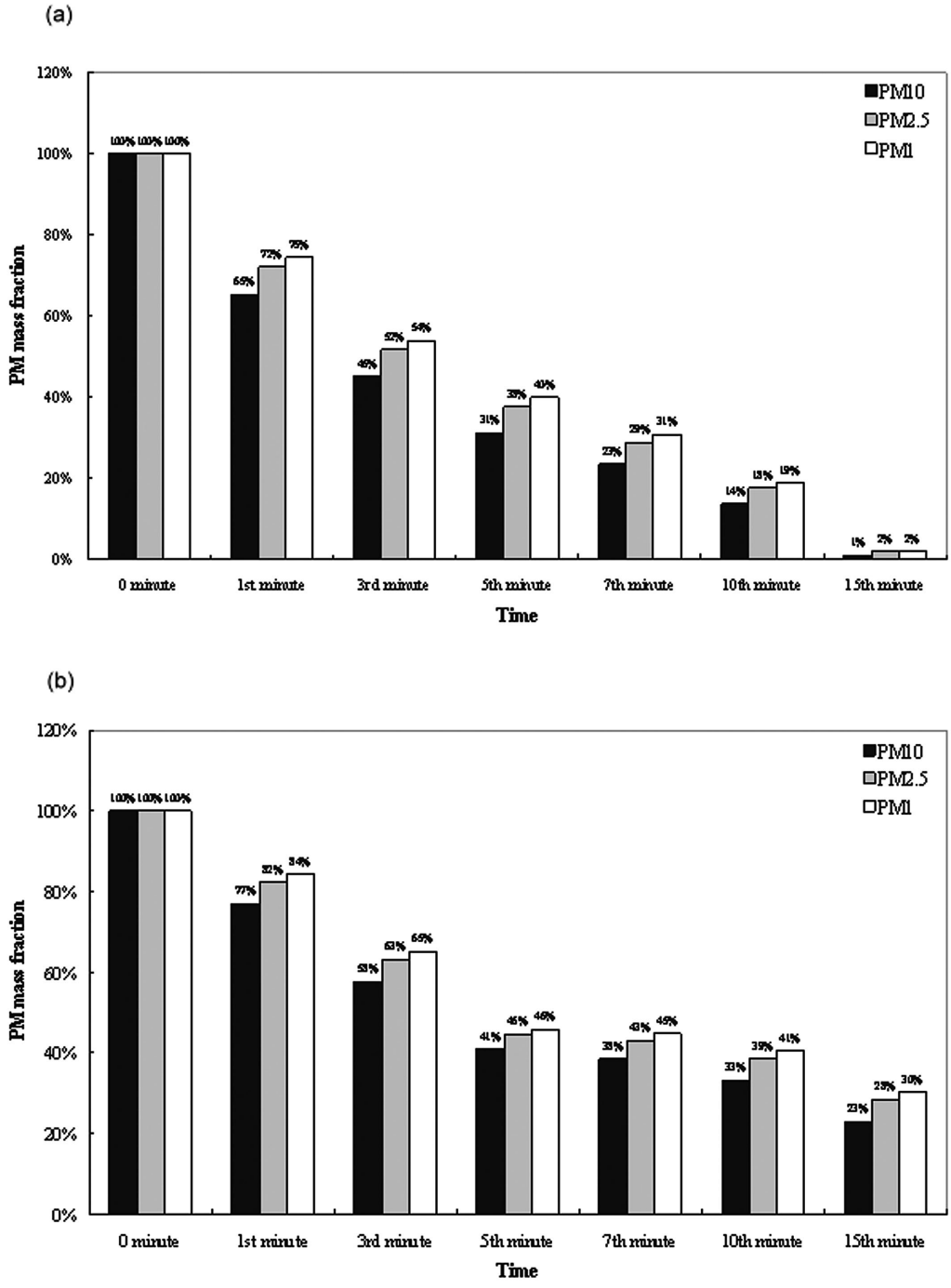

Figure 7. Time variations of the canopy-averaged mass concentrations of PM_{10}, $PM_{2.5}$, and PM_1 in the (a) open and (b) staggered street canopies.

validated upon data of the wind tunnel experiments, but the results of particle transport calculations were not validated. The real atmospheric conditions in urban streets are more complicated than our study cases. It is hoped that the study presented here can be a stimulus for experimenters to conduct additional laboratory and field experiments and to compare their findings with our numerical results.

CONCLUSIONS

On the basis of the simulated results, the research presented here has led to the following conclusions:

(1) A size-dependent PM transport model, adopting the Eulerian LES of turbulent flow and the Lagrangian particle trajectory tracking, has been verified by the reliable experimental measurement. It is an effective method to investigate the complicated canopy flow patterns and $PM_{10}/PM_{2.5}/PM_1$ transport mechanisms in the street canopies.

(2) For the open street canopies, particles are effectively driven by unimpeded canopy flows from the upwind to downwind buildings. All PM_{10}, $PM_{2.5}$, and PM_1 mass concentrations are substantially reduced. However, in the case of the staggered street

canopies, the unimpeded canopy airflow only occurs in the first column of the buildings. All PM_{10}, $PM_{2.5}$, and PM_1 removals are less effective. As a result, the open street canopies having higher PM removal ability lead to a swifter shift of the particle size distributions towards smaller size and less deviation than the staggered street canopies.

(3) Whether in the open or staggered street canopies, PM_{10} is easier to remove compared with $PM_{2.5}$ and PM_1. This phenomenon is responsible for the fact that fine particles are more influenced by the canopy airflows, resulting in more accumulation of $PM_{2.5}$ and PM_1 within urban street canopies than PM_{10}. Thus, from the purpose of health protection for urban passengers, using PM_{10} level as the only PM index is not enough. $PM_{2.5}$ and PM_1 levels should also be considered.

(4) Particle escape is the most important removal mechanism for the open street canopies, whereas wall deposition is the major removal mechanism for the staggered street canopies.

ACKNOWLEDGMENTS

The authors gratefully acknowledge support of this work by a 3-yr project of the National Science Council, Taiwan, Republic of China, under Grant Nos. NSC 95-2625-Z-002-025, 96-2625-Z-002-014, and 97-2625-M-002-003.

REFERENCES

1. Pope, C.; Burnett, R.; Thun, M.; Calle, E.; Krewski, D.; Ito, K.; Thurston, G. Lung Cancer, Cardio-Pulmonary Mortality, and Long-Term Exposure to Fine Particulate Air Pollution; *J. Am. Med. Assoc.* **2002**, *287,* 1132-1141.
2. Penttinen, P.; Timonen, K.L.; Tiittanen, P.; Mirme, A.; Ruuskanen, J.; Pekkanen, J. Ultrafine Particles in Urban Air and Respiratory Health among Adult Asthmatics; *Eur. Respir. J.* **2001**, *17,* 428-435.
3. Dockery, D.W.; Pope, C.A. Acute Respiratory Effects of Particulate Air Pollution; *Ann. Rev. Pub. Health* **1994**, *15,* 107-132.
4. Anderson, P.J.; Wilson, J.D.; Hiller, F.C. Respiratory Tract Deposition of Ultrafine Particles in Subjects with Obstructive or Restrictive Lung Disease; *Chest* **1990**, *97,* 1115-1120.
5. Harrison, R.M.; Yin, J. Particulate Matter in the Atmosphere: Which Particle Properties are Important for Its Effects on Health?; *Sci. Total Environ.* **2000**, *249,* 85-101.
6. Hitchins, J.; Morawska, D.; Gilbert, D.; Jamriska, M. Dispersion of Particles from Vehicle Emission around High- and Low-Rise Buildings; *Indoor Air* **2002**, *12,* 64-71.
7. Berkowicz, R. Using Measurements of Air Pollution in Streets for Evaluation of Urban Air Quality-Meteorological Analysis and Model Calculations; *Sci. Total Environ.* **1996**, *189/190*, 259-265.
8. Xie, S.; Zhang, Y.; Qi, L.; Tang, X. Spatial Distribution of Traffic-Related Pollutant Concentrations in Street Canyons; *Atmos. Environ.* **2003**, *37,* 3213-3224.
9. Sagrado, A.P.G.; Beeck, J.V.; Rambaud, P.; Olivari, D. Numerical and Experimental Modeling of Pollutant Dispersion in a Street Canyon; *J. Wind Engineer. Indust. Aerodynam.* **2002**, *90,* 321-339.
10. Ahmad, K.; Khare, M.; Chaudhry, K.K. Wind Tunnel Simulation Studies on Dispersion at Urban Street Canyons and Intersections—a Review; *J. Wind Engineer. Indust. Aerodynam.* **2005**, *93,* 697-717.
11. Mfula, A.M.; Kukadia, R.F.; Griffiths, R.F.; Hall, D.J. Wind Tunnel Modeling of Urban Building Exposure to Outdoor Pollution; *Atmos. Environ.* **2005**, *39,* 2737-2745.
12. Walton, A.; Cheng, A.Y.S. Large-Eddy Simulation of Pollution Dispersion in an Urban Street Canyon. Part II: Idealized Canyon Simulation; *Atmos. Environ.* **2002**, *36,* 3615-3627.
13. Walton, A.; Cheng, A.Y.S.; Yeung, W.C. Large-Eddy Simulation of Pollution Dispersion in an Urban Street Canyon. Part I: Comparison with Field Data; *Atmos. Environ.* **2002**, *36,* 3601-3613.
14. Caton, F.; Britter, R.E.; Dalziel, S. Dispersion Mechanisms in a Street Canyon; *Atmos. Environ.* **2003**, *37,* 693-702.
15. Lee, I.Y.; Park, H.M. Parameterization of the Pollutant Transport and Dispersion in Urban Street Canyons; *Atmos. Environ.* **1994**, *28,* 2343-2394.
16. So, E.S.P.; Chan, A.T.Y.; Wong, A.Y.T. Large-Eddy Simulations of Wind Flow and Pollutant Dispersion in a Street Canyon; *Atmos. Environ.* **2005**, *39,* 3573-3582.
17. Xie, X.; Huang, Z.; Wang, J.; Xie, Z. The Impact of Solar Radiation and Street Layout on Pollutant Dispersion in Street Canyon; *Atmos. Environ.* **2005**, *40,* 201-212.
18. Xia, J.Y.; Leung, D.Y.C. Pollutant Dispersion in Urban Street Canopies; *Atmos. Environ.* **2001**, *35,* 2033-2043.
19. Chang, T.J.; Wu, Y.T. Wind-Driven Rain Distributions around Street Canopies; *J. Am. Water Res. Assoc.* **2003**, *39,* 545-562.
20. Liu, C.; Ahmadi, G. Computer Simulation of Pollutant Transport and Deposition near Peace Bridge; *Particulate Sci. Technol.* **2005**, *23,* 109-127.
21. Ahmadi, G.; Li, A. Computer Simulation of Particle Transport and Deposition near a Small Isolated Building; *J. Wind Engineer. Indust. Aerodynam.* **2000**, *84,* 23-46.
22. Hanna, S.R.; Tehranian, S.; Carissimo, B.; Macdonald, R.W. Comparisons of Model Simulations with Observations of Mean Flow and Turbulence within Simple Obstacle Arrays; *Atmos. Environ.* **2002**, *36,* 5067-5079.
23. Cheng, Y.; Lien, F.S.; Yee, E.; Sinclair, R. A Comparison of Large Eddy Simulations with a Standard k-ε Reynolds-Averaged Navier-Stokes Model for the Prediction of a Fully Developed Turbulent Flow over a Matrix of Cubes; *J. Wind Engineer. Indust. Aerodynam.* **2003**, *91,* 1301-1328.
24. Zhang, A.; Gao, C.; Zhang, L. Numerical Simulation of the Wind Field Around Different Building Arrangements; *J. Wind Engineer. Indust. Aerodynam.* **2005**, *93,* 891-904.
25. Ferziger, J.H.; Peric, M. *Computational Methods for Fluid Dynamics*, 3rd ed.; Springer: Berlin, 2002.
26. Smagorinsky, J. General Circulation Experiments with the Primitive Equations. I. The Basic Experiment; *Mon. Weather Rev.* **1963**, *91,* 99-164.
27. Ciofalo, M. Large-Eddy Simulations of Turbulent Flow with Heat Transfer in Simple and Complex Geometries Using Harwell-Flow3D; *Appl. Math. Model.* **1996**, *20,* 262-271.
28. Chang, T.J.; Hsieh, Y.F.; Kao, H.M. Numerical Investigation of Airflow Pattern and Particulate Matter Transport in Naturally Ventilated Multi-Room Buildings; *Indoor Air* **2006**, *16,* 136-152.
29. Chang, T.J.; Kao, H.M.; Hsieh, Y.F. Numerical Study of the Effect of Ventilation Pattern on Coarse, Fine, and Very Fine Particulate Matter Removal in Partitioned Indoor Environment; *J. Air & Waste Manage. Assoc.* **2007**, *57,* 179-189.
30. Chang, T.J.; Yen, B.C. Gravitational Fall Velocity of Sphere in Viscous Fluid; *J. Engineer. Mech. ASCE* **1998**, *124,* 1193-1199.
31. Li, A.; Ahmadi, G. Dispersion and Deposition of Spherical Particles From Point Sources in a Turbulent Channel Flow; *Aerosol Sci. Technol.* **1992**, *16,* 209-226.
32. Chang, T.J.; Hu, T.S. Transport Mechanism of Airborne Particulate Matter in Partitioned Indoor Environment; *Building & Environ.* **2008**, *43,* 886-895.
33. Hinds, W.C. *Aerosol Technology: Properties, Behavior, and Measurement of Airborne Particles*, 2nd ed.; John Wiley & Sons: New York, 1999.
34. Meinders, E.R.; Hanjalic, K. Vortex Structure and Heat Transfer in Turbulent Flows over Wall-Mounted Matrix of Cubes; *Int. J. Heat Fluid Flow* **1999**, *20,* 255-267.
35. Macdonald, R.W.; Carter, S.; Slawson, P.R. *Measurements of Mean Velocity and Turbulence Statistics in Simple Obstacle Arrays at 1:200 Scale*; Thermal Fluids Report 2000-1; Department of Mechanical Engineering; University of Waterloo: Waterloo, Ontario, Canada, 2000.

About the Authors

Tsang-Jung Chang is a professor in the Department of Bioenvironmental Systems Engineering, National Taiwan University, Taipei, Taiwan, Republic of China. Hong-Ming Kao is a Ph.D. student and Yu-Ting Wu and Wei-Hua Huang are former graduate students in the same department. Yu-Ting Wu is currently a Ph.D. student in the Department of Civil Engineering, University of Minnesota, Minneapolis, MN. Wei-Hua Huang is an engineer in Taiwan Semiconductor Manufacturing Co. Ltd., Hsinchu, Taiwan. Please address correspondence to: Tsang-Jung Chang, Department of Bioenvironmental Systems Engineering, National Taiwan University, 1, Section 4, Roosevelt Road, Taipei 106, Taiwan, Republic of China; phone: +886-2-23622977; fax: +886-2-23635854; e-mail: tjchang@ntu.edu.tw.